Impact of gravity on directional solidification of refined Al-20wt.%Cu alloy investigated by in situ X-radiography

Hadjer Soltani, Fabiola Ngomesse, Guillaume Reinhart, Mohamed Chérif Benoudia, Moussa Zahzouh, Henri Nguyen-Thi

Impact of gravity on directional solidification of refined Al-20wt.%Cu alloy investigated by *in situ* X-radiography

Hadjer Soltani [a,c], Fabiola Ngomesse[a], Guillaume Reinhart [a], Mohamed Chérif Benoudia[b], Moussa Zahzouh[c] and Henri Nguyen-Thi [a]

[a] Aix Marseille University, CNRS, IM2NP, UMR 7334, Marseille, France

[b] Ecole Nationale supérieure des Mines et de la Métallurgie, L3M, Annaba, Algeria

[c] Badji Mokhtar University, LMGM, BP 12, 23000, Annaba, Algeria

Abstract

Gravity effects such as natural convection in the liquid phase and buoyancy forces acting on the solid phase have a strong influence on the grain structure and microstructure formation dynamics during the solidification of metal alloys. It is thus very useful to undertake experimental studies that will provide benchmark data for a deeper understanding of the role of such gravity effects. In this paper, we study the formation of the equiaxed grain structure during refined Al-20wt.%Cu solidification in a temperature gradient for three different configurations: horizontal, vertical upward and vertical downward solidification. The key grain characteristics, namely grain size, grain elongation and grain growth orientation, were determined for all experiments and a comparative study was performed to identify the dominant effects of gravity

for each case. The present study provides quantitative information on the impact of grain flotation and solute flows on the equiaxed microstructure characteristics by means of *in situ* laboratory X-radiography.

Keywords: Directional solidification, equiaxed microstructure, grain characteristics, *in situ* X-radiography, Al-Cu alloy, gravity, convection, buoyancy

1. Introduction

Metal material properties such as ductility and hardness are closely linked to the grain structure generated during solidification processes. Ever better understanding of grain structure dynamics during its development and of related underlying mechanisms is thus of utmost importance to control the growth conditions for engineering applications and to obtain pieces with the desired and reproducible properties. During solidification in a temperature gradient, two types of grain structure can form depending on the growth conditions (alloy composition, temperature gradient and cooling rate or sample pulling velocity): the columnar grain structure, with directional properties and the equiaxed grain structure with more uniform and isotropic properties. The equiaxed grain structure is the most used in aluminium-based industrial applications and can be promoted by inoculation, which consists in adding inoculant particles to the melt. These micrometer particles act as preferential sites for heterogeneous nucleation of α-Al grains, resulting in a uniformly fine, equiaxed as-cast microstructure [1, 2]. The same principle is also successfully applied to other metallic systems, notably magnesium and zinc alloys.

On Earth, gravity has a strong impact on the formation of solidification microstructures and makes the study of alloy solidification more complex because of the combination of multiple phenomena at different scales in time and space. Firstly, natural convection takes place in the melt and is the major source of various disturbing effects, which can significantly modify or mask other physical mechanisms [3-7]. Indeed, flows in the liquid modify the solute transport

47 in the melt, and generally prevent the formation of steady solidification patterns with uniform
48 features. Thus, attempts have often been made to avoid convection in the melt in directional
49 solidification studies to make easier the interpretation of the results [8]. A simple way of
50 eliminating or reducing natural convection is to ensure that the density gradient in the liquid
51 phase is vertical downward everywhere, the heavier liquid being at the bottom. This situation
52 is more or less approached when growth occurs in a vertical upward temperature gradient, for
53 an alloy system in which the rejected solute is denser than the solvent. For example, this is the
54 case during upward directional solidification of hypo-eutectic Al-Cu alloys. However, even in
55 this configuration, flow patterns adjacent to the solid-liquid interface can develop at low growth
56 rates under the effect of a transverse horizontal temperature gradient that exists because of the
57 difference in thermal conductivities of the solid phase, liquid phase and crucible wall. In that
58 specific case, fluid flows can cause strong deformation (steepling and clustering phenomena)
59 of the solid-liquid interface [9-11] and then large segregation in the material [12, 13]. For
60 vertical downward solidification of hypo-eutectic Al-Cu alloys, both thermal and solutal
61 gradients destabilize the liquid phase and strong convective motion in the melt are expected
62 that can modulate macroscopically the solid – liquid interface, can delay or activate the
63 morphological stability of the solid – liquid interface, and also leads to a significant longitudinal
64 (parallel to the growth direction) macro-segregation [11, 14].
65 For vertical solidification experiments, regardless of the growth direction (upward or
66 downward), an additional effect of gravity is buoyancy that acts on solid elements like dendrite

fragments and free grains. This force provokes either grain sedimentation or flotation, depending on the relative densities of the grain and the surrounding liquid [15-17]. It is worth noticing that buoyancy force acting on secondary dendrite arms also induces dendrite bending, leading in some cases to dendrite fragmentation [18].

Diffusive mass transport without any buoyancy effect can be achieved during microgravity experiments [17, 19-23], independently of alloy composition and container shape. However, such type of experiments is rare and very expensive, because of the limited number of microgravity opportunities. In normal gravity conditions, nearly diffusive conditions can be achieved by performing horizontal solidifications of very thin samples (down to 10 µm in thickness), like in the case of transparent alloys solidification experiments [8]. In this experimental configuration, fluid flows are blocked by the strong confinement in one dimension. For metallic samples, it is very difficult to reduce the thickness down to 10 µm in a uniform way and typical sample thickness is in the range 100-300 µm. For this value, natural convection [17] and buoyancy effects [24] during horizontal solidification are largely, but not completely, reduced.

It is now well established that *in situ* and time-resolved study of solidification is relevant because most of the phenomena that occur during the process are dynamic. Various X-ray imaging methods have been developed in the last two decades, in particular using synchrotron radiation [25]. However, *in situ* X-radiography remains the most used method for studying metal alloy solidification because of its simplicity. X-radiography enables us to follow the

dynamics of the solid-liquid interface [26], the grain motion [27-29] and under certain conditions to determine quantitatively the solute concentration in the liquid phase [30, 31]. In the last decade, benefitting from the progress of microfocus X-ray sources and detectors, laboratory [32-35] as well as microgravity [17, 24, 36] apparatus have been developed to study *in situ* the solidification of metals. Even if microfocus X-ray sources do not generate a beam as powerful as synchrotron sources, they offer enough brilliance to conduct investigations of Al-based alloy solidification.

The aim of the present investigation is to examine and enlighten the major effects of gravity during the formation of an equiaxed microstructure in a fixed temperature gradient. For this purpose, directional solidifications of refined Al-20%Cu samples were carried out with different orientations of the sample with respect to the gravity direction, namely horizontal and vertical (upward and downward) solidifications. Experiments were performed in the SFINX (Solidification Furnace with IN Situ X-radiography) laboratory facility, which enabled us to follow the formation of the equiaxed microstructure using *in situ* X-radiography. The main grain and microstructure characteristics have been determined for all the experiments. Then, a comparative analysis between the various configurations has been conducted to emphasize the impact of natural convection as well as buoyancy force acting on the grains after nucleation during the formation of the equiaxed microstructure.

2. Experiment description

2.1. SFINX apparatus

Directional solidification experiments were performed in the SFINX (Solidification Furnace with IN Situ X-radiography) laboratory device, which is a duplicate of the facility used during several parabolic flight campaigns [36] as well as during the sounding rocket experiment MASER-12 [17]. These facilities were developed within the ESA (European Space Agency) project entitled XRMON (X-ray MONitoring of advanced metallurgical processes under terrestrial and microgravity conditions) to study the microstructure formation dynamics of metal alloys onboard of microgravity platform using X-radiography [37]. A detailed description of those facilities has been given in our previous papers [17, 19]. Only the main features are summarized below.

The dimensions of the sheet-like samples of refined Al-20wt.%Cu (0.1wt.%AlTiB) were 5 mm in width, 50 mm in length and 0.25 mm in thickness. The sample thickness was chosen in order to have a good transmission of the X-ray beam and prevent the superimposing of several grains at the same location so that the interpretation of radiographs is unambiguous. The polished sample was placed into stainless-steel spacers, sandwiched between two flexible glassy carbon sheets sewn together with a silica thread. The sample-crucible assembly was then installed inside the Bridgman-type furnace (Fig. 1a). The furnace consists of two identical heaters for the "hot" and "cold" zones that are independently regulated by a PID-regulator. During the experiments, the samples were directionally solidified by applying the same cooling rate R on

127 both heater elements, ensuring a fixed temperature gradient *G* during the entire experiment. The
128 furnace enables directional solidification with temperature gradients within the range of 2.5-15
129 K/mm and cooling rates *R* within the range of 0.01–1.5 K/s.

130 The X-radiography system features a microfocus X-ray source with a molybdenum target
131 and a 3 mm focal spot (Fig. 1b). It provides a photon flux with two peaks of energy at 17.4 keV
132 and 19.6 keV that ensure a good image contrast to study Al-Cu based alloys. The camera system
133 is made of a scintillator plate that converts X-ray radiation to visible light and a digital camera
134 with a CCD-sensor. As a result of the X-ray beam divergence, a geometric magnification of the
135 object is observed at the detector, which is the ratio of the source-detector to source-object
136 distances, the object in this case being the sample. In this work a magnification of ~5 was
137 obtained for a Field-of-View (FoV) of about 5x5 mm^2 and an effective pixel size of ~4x4 μm^2.
138 The acquisition rate was 2 frames/second.
139 Grey level variations in the radiographs are related to the difference in X-ray absorption of the
140 different parts of the sample, which depends mainly on the local density and composition.
141 Image quality was enhanced by applying an image processing consisting in dividing each
142 recorded frame by a reference picture recorded just before the beginning of the solidification
143 [38]. After image processing, radiographs showed the equiaxed grains microstructure formed
144 during the directional solidification of the refined Al-20wt.%Cu. Liquid regions of high copper
145 concentration showed up as dark regions in the images, while α-Al dendritic grains with low
146 copper concentration were discernible as bright regions in the FoV [27, 30].

2.2. Experimental configurations

For comparison purposes, four refined Al-20wt.%Cu specimens were solidified with similar experimental parameters but with different orientations of the gravity vector. The furnace was set in two positions, allowing us to perform directional solidification experiments in three different configurations with respect to gravity: horizontal (1 sample), vertical upward (2 samples) and vertical downward (1 sample).

- *Case A*: the main surface of the sample was set perpendicular to the gravity vector ***g*** (Fig. 1b) and the solidification of the sample took place horizontally. In this experimental arrangement, the effects of gravity are expected to be strongly minimized.
- *Case B*: the samples were set in a vertical position by rotating the whole SFINX apparatus and the temperature gradient is anti-parallel to ***g*** (bottom-up growth). During upward solidification of refined Al-20wt.%Cu alloy, both thermal and solutal gradient are stabilizing and natural convection is mainly due to the residual transverse temperature gradient [9, 10, 13]. Moreover, the impact of buoyancy on equiaxed grains will push the aluminum grains upward [28].
- *Case C*: with the same furnace position as in *Case B*, downward solidification of the sample was performed with a temperature gradient parallel to the gravity vector (top-down growth). In this case, both thermal and solutal gradients are destabilizing and strong convective flows are expected.

2.3. Solidification parameters

We solidified the refined Al-20wt.%Cu specimens in different gravity conditions, as described in the previous section, and with close growth parameters. Table 1 summarizes the growth parameters of the experiments presented in this paper. The cooling rate value was identical for all the experiments, R = 0.15 K/s, but the temperatures of the heater elements had to be adjusted for each configuration to achieve nearly the same average growth velocities and temperature gradients. Indeed, because of the asymmetry of the sample holder design as visible in Fig. 1a [19], the temperature interval between the two heater elements had to be increased by a factor two for the upward solidification experiments to obtain the same temperature gradient in the sample than for horizontal or downward solidifications. Furthermore, experiments with the same control parameters were carried out several times for each configuration to check the repeatability of the experiments and to improve our statistical analysis in terms of grain size, grain elongation and grain orientation (cf. section 2.4).

To determine accurate values of the growth parameters, we developed an experimental procedure based on the radiographs to measure in a first step the growth velocity [39]. The position of each grain in the FoV was marked manually as soon as they became visible (diameter ≥ 10-20 µm) and the corresponding time was recorded. Then, the positions of the nucleation events were plotted as a function of time, and the average nucleation front velocity $\langle V_N \rangle$ can be easily derived from this plot. Assuming that the grain nucleation always occurs at a temperature close to the liquidus temperature in the case of refined alloys [40], the nucleation

front velocity was considered similar to the liquidus temperature velocity. The nucleation front velocity can be compared to the velocity of the eutectic front $<V_E>$ that crossed the FoV at the end of the solidification phase. A good agreement was obtained between the two types of measurement (see Table 1). Hereafter, the average nucleation front velocity $<V_N>$ will be used to compare the different experiments. In a second step, the actual temperature gradient was calculated using the relation $G = R/V$, which was assumed to be valid in our experiments.

2.4. Grain structure characterization

A dendritic equiaxed microstructure was obtained during the cooling of the samples due to the AlTiB refining particles added into the alloy. By using X-radiography, the solidification was observed *in situ* with the equiaxed grain structure propagating from the cold zone to the hot zone. For each different configuration (horizontal, vertical upward and vertical downward solidifications), significant differences were observed for the solidification process as will be presented in the next sections. To analyze the gravity effects on the final grain structure, a quantitative analysis was conducted to determine the distribution of grain size, elongation and growth orientation for all experiments. The *in situ* observation of the solidification process allowed us to follow the microstructure formation and thus to measure the grain characteristics without any ambiguity. The first step consisted of contouring the grains one by one with the free software ImageJ [41] in order to obtain the grain surface area, using a semi-automatic macro script [39]. It was then possible to determine the distributions of grain size, grain

elongation and grain growth orientation:

- The grain size is defined as the diameter d of a disk having the same grain surface area, named equivalent disk (white circle in Fig. 2a). The grain surface area is easily retrievable since it is given by the ImageJ software in pixels. Even if the grain size is a very important parameter, it gives no information about the grain morphology and must be completed by other measurements.
- The grain elongation factor ϕ is defined in a classical way by $\phi = L_1/L_2$, with L_1 being the length of the longest straight segment inscribed within the grain and L_2 the length of the longest straight segment inscribed within the grain and orthogonal to the segment that gives L_1 (Fig. 2b). Both L_1 and L_2 were automatically obtained from the grain contouring using a macro in ImageJ. This definition is the inverse of the one used by Biscuola and Martorano [42] and the elongation factor varies in our paper from unity (for a perfectly equiaxed grain) to larger values (up to ten) for elongated grains.
- The growth orientation of each grain with respect to the temperature gradient direction was also measured. This grain orientation is characterized by the tilt angle θ between the temperature gradient direction and the main dendrite axis (Fig. 2c). This third grain parameter is important to measure the impact of the temperature gradient on the growth direction. A wide θ-distribution around a zero average value means that there is no preferential direction for the grain growth and thus that there is no influence of the temperature gradient on the grain growth direction.

227 It is worth noticing that similar information could be obtained by post-mortem microscopy,
228 but only for the last solidification experiment since the samples were melted in between each
229 solidification sequence.
230
231 **3. Case A: horizontal solidification**
232 **3.1. Formation of the equiaxed grain structure**
233 Fig. 3 shows a sequence of radiographs recorded during the experiments labelled A1 carried
234 out in horizontal configuration. The solidification started with a fully melted sample and the
235 application of the cooling rate on both heaters of the gradient furnace gave rise to the formation
236 of grains in the cold zone of the furnace (Fig. 3a). Then, the solidification front propagated by
237 wave-like nucleation ahead of the solidification front, in a similar way to the observations
238 reported by many authors [43-46]. After their nucleation, the grains developed from almost the
239 same initial location in the radiographs (Fig. 3a). By looking carefully at the grain dynamics, it
240 was seen that some grains slightly rotated and seemed to move in the sample thickness. Many
241 grains slightly moved towards the cold part of the sample due to solidification-induced
242 shrinkage and interdendritic flow of the liquid phase as reported by Salloum et al. [28] for
243 dendrite fragments. Those effects induced only very small grain motions and did not affect the
244 key grain structure parameters. The entire solidification process can be seen in Supplementary
245 Video 1.
246 After a short stage of rapid growth, the grains interacted with each other and gradually

247 formed a compact grain structure for which it was possible to define an effective front, at the
248 top of the grain network (dashed line in Fig. 3c). This effective front separated the upper limit
249 of the developing grain structure and the fully liquid phase. As the cooling of the sample
250 continued, new layers of grains nucleated in the undercooled liquid zone ahead of the effective
251 front (Fig. 3c). The new grains grew and eventually blocked the advancing effective front before
252 being incorporated into the grain compact structure to form a new effective front. This
253 mechanism was repeated over time (Fig. 3d), which lead to the formation of the equiaxed
254 structure until the complete filling of the FoV (Fig. 3e). It is worth noticing that the grains were
255 more elongated at the top of the FoV than in the bottom part. This was due to a higher
256 longitudinal temperature gradient in this region close to the hot heater element of the furnace
257 [39]. The remaining intra- and inter-dendritic liquid areas solidified at a later stage, following
258 the crossing of the eutectic front through the FoV (dotted line in Fig. 3f).
259
260 **3.2. Grain structure characterization**
261 In Case A (horizontal solidification), the final grain structure in the FoV was composed of
262 rather homogeneous and well dispersed grains. This was confirmed by the distributions of grain
263 diameter (Fig. 4a), grain elongation factor (Fig. 4b) and grain growth orientation (Fig. 4c) for
264 the experiment A1, which agrees with a recent detailed analysis of the impact of growth velocity
265 on those distributions for a similar experimental configuration [39, 47]. The distribution of grain
266 diameter was well-fitted by a Gaussian-type curve and the microstructure was rather

homogeneous in size in the FoV. For the grain size, the mean and maximal values were about $d_{peak} \sim 520$ µm and the width at half height was $\sigma = 170$ µm (similar values were obtained for experiment A2). For the elongation factor, the distribution was well-fitted by a log-normal type curve, as shown in Fig. 4b. It can be seen that the largest number of grains had an elongation factor ϕ lower than two (the maximum ϕ_{peak} is about 1.4, with a width at half height σ=0.4), which means that the grain structure was of equiaxed type, according to Hunt criterion [48]. A more detailed analysis of this histogram confirmed that the rare elongated grains ($\phi > 2$) were mainly located in the top part of the FoV, in the region close to the hot heater element of the furnace where the temperature gradient was larger. Finally, the grain orientation distribution (Fig. 4c) was rather wide, with a peak at an angle $\theta_{peak} \sim 9°$, which indicates that the grain orientation was not completely random as would have been expected for a perfectly equiaxed grain structure. The growth orientation was still influenced by the temperature gradient along the sample in these directional solidification experiments, as recently shown by H. Soltani *et al.* [39].

4. Case B: Upward solidification

4.1. Impact of buoyancy on grain structure formation

A sequence of radiographs recorded during the upward solidification experiment labelled B2 is shown in Fig. 5. The solidification parameters of this experiment were close to those of the experiment A1 described in the previous section (Table 1). The major difference between Case B and Case A was the impact of buoyancy force that induced the flotation of grains after

their nucleation (see Supplementary Video 2), due to the difference of densities between the solid and the liquid, the aluminum grains being much lighter than the surrounding Cu-rich liquid for equiaxed solidification of Al-20wt.% Cu alloys [49].

Because of buoyancy forces acting on all the nucleated grains, two different types of behavior were observed during the cooling of the sample. Firstly, some grains moved towards the hot part of the sample where they gradually melted, as described in detail in [28, 36] and clearly visible in the earlier stage of the experiment when there is still no well-defined equiaxed microstructure in the FoV. The upward motion of some grains is indicated by white arrows in Fig. 5a and this phenomenon can be seen more clearly in Supplementary Video 2. The second type of grain behavior is specific to experiments carried out in thin samples (about 200 µm in thickness). Due to the strong confinement, the upward motion of some grains could be stopped when their size was of same order than the sample thickness. When this occurred, they continued to develop roughly at the same location, like the pair of grains in plain circles in Fig. 5b that remain visible in the subsequent radiographs. This “move-and-stop” behavior had two important effects on the final grain structure. Firstly, large residual liquid areas (rich of Cu) were forming in between the grains and lead to segregated regions like the one pointed out in Fig. 5b and Fig. 5d. Subsequently, a few new grains nucleated in the residual liquid areas and moved upward until they were blocked by the previously stuck grains. The possibility of grain nucleation between growing grains has also been recently reported by Jia *et al.* during refined Al-15wt.%Cu alloy solidification [46]. In addition, another effect induced by gravity during

upward solidification was the promotion of dendrite fragmentations [50], leading to the development of many small grains inside the already grown microstructure.

4.2. Grain structure characterization

Grain size distribution, grain elongation factor and growth orientation angle are depicted in Fig. 6. Despite the impact of buoyancy forces acting on solid grains, the grain size distribution remained gaussian, with a peak value at about 520 µm, which is surprisingly the same value than in the case of horizontal solidification. However, the width at half height was σ = 260 µm, which is much larger than for horizontal solidification (σ = 170 µm). For this experimental configuration, grains remained of equiaxed-type as shown by Fig. 6b, with ϕ_{peak} = 1.3, also close to the value of the horizontal case. The grain orientation distribution is wide, with a peak value at θ = 8°, which confirms that there is still a preferred grain orientation parallel to temperature gradient direction, despite the random motion and rotation of the equiaxed grains when floating.

5. Case C: Downward solidification

5.1. Solute plumes observations

For vertical downward solidification, the temperature gradient was parallel to the gravity vector, so that the temperature field was destabilizing regarding convective instabilities as the hot liquid was below the cold liquid. Moreover, the rejected solute (Cu) is heavier than the solvent (Al) yielding the solute to sink due to gravity and amplifying convective flow.

329 Thermosolutal convection is then expected to be the dominant gravity-driven effect in this case.
330 Fig. 7 depicts a sequence of radiographs of the experiment C1, showing the representative
331 behaviour of all downward solidification experiments. In this experiment, an initially small
332 porosity defect (≈ 80 µm in diameter) developed into a larger hole (around 500 µm in width)
333 visible at the bottom of the FoV as indicated in the first radiograph in Fig. 7a. The entering of
334 the first grains in the FoV from the cold region of the sample is also visible Fig. 7a, as well as
335 downward flows of Cu-rich liquid coming from the solidification microstructure and moving
336 towards the bulk liquid (white arrows). These flows, also called convective plumes, were visible
337 long before the appearance of the first grains in the FoV (readers are encouraged to see the
338 Supplementary Video 3) and are caused by the rejection of heavy solute in the mushy zone
339 during the solidification microstructure formation. In the radiographs, these plumes are visible
340 because they are solute-rich and thus their X-ray absorption differs from the surrounding liquid
341 at nominal composition.
342 Like in the previous experiments, the solidification microstructure progressed toward the
343 hot part of the sample by wave-like nucleation mechanism. However, due to buoyancy force,
344 the new solid grains floated and moved back against the existing solidification front and thus
345 stopped rapidly the growth of existing grains (Fig. 7b to Fig. 7e). Accordingly, the equiaxed
346 grains formed a dense and compact microstructure, whose characteristics were very different
347 from the horizontal or upward solidification experiments due to gravity effects as discussed
348 later in section 5.3. During the propagation of the solidification front, the plumes were drifting

continuously along the existing microstructure, as clearly visible in Supplementary Video 3. Interestingly, solidification was delayed at the root of the segregated channel due to the local increase of solute composition (Fig. 7b, 7c and 7d). The remelting of some small grains entering the Cu-rich channel was also observed (see Supplementary Video 3).

5.2. Interaction between solute plumes and dendrite growth

The impact of solute plumes on dendrite growth kinetic has been analyzed by means of X-radiography visualization. Using the ImageJ software, we were able to measure *(i)* the tip position of several dendrites and then to deduce their growth velocities as a function of time and *(ii)* the gray level in front of the dendrite tip. In our experiments, it was not possible to convert in a straightforward manner the gray level into solute concentration. However, the gray level values are related to the liquid concentration in front of the dendrite tip: the lower the gray level, the higher the liquid composition.

The studied dendrites were selected according to their growth direction, parallel to both gravity and temperature gradient, and their growth duration. For all the measured dendrites, it has been found that the dendrite tip velocity was strongly influenced by solute plumes passing in front of them, as illustrated in Fig. 8. For the dendrite indicated in Fig. 8a, we had the opportunity to reveal up clearly the interaction between the solute variation induced by solute plumes flows (Fig. 8b) and the dendrite tip growth velocity (Fig. 8c). In fact, the dendrite tip growth velocity oscillated above and below an average value, with a period of ≈ 20 seconds,

showing marked minimum and maximum. Comparing the two plots in Fig. 8 highlighted the close relationship between the dendrite tip growth velocity and the gray level variation. The variations of the dendrite tip velocity were approximately in phase with the liquid solute composition variations, i.e. the minimum and maximum of both curves occurred roughly simultaneously (as indicated by the dashed lines connecting the two curves). A maximum of Cu concentration in front of the dendrite tip gave a minimum of dendrite tip velocity. Moreover, in addition to the remarkable synchronization of these two curves, the oscillation amplitude variations were also in close accordance, at least qualitatively.

5.3. Grain structure characterization

When visually comparing the grain structure for Case C (downward solidification) with both other cases, the microstructure was found more compact, with both smaller and more elongated grains than for the horizontal and vertical upward solidifications.

Fig. 9a depicts the grain diameter distribution, which was not of gaussian type but well fitted by a log-normal function. The peak value for this experiment was about 184 µm, which is nearly three times smaller than the value of the gaussian function of Case A or the average arithmetic mean of Case B. This log-normal distribution means that the grain structure was mainly composed of small grains completed by some longer grains. The more columnar aspect of the grain structure was confirmed by (*i*) the distribution of the elongation factor (Fig. 9b) that showed that the number of grains with an elongation factor higher than 2 was higher than

for horizontal or upward case and (*ii*) the distribution of tilt angle (Fig. 9c) that is of gaussian type with a prominent maximum close to 0°.

6. Discussion

The investigation of solidification experiments carried out with different orientations of the sample with respect to the gravity vector is an effective approach to highlight the impact of gravity-related phenomena on the solidification microstructure formation. Comparing vertical upward and downward experiment allows the impact of convective flow and buoyancy to be studied in thermo-solutally stabilizing or destabilizing configurations, as recently illustrated by Nelson *et al.* using *in situ* 4D synchrotron tomography for the solidification of an Al-15wt.%Cu alloy [51]. Valuable information can be obtained when such results are complemented by reference experiments performed in diffusive conditions, such as microgravity environment, as clearly demonstrated by Dupouy *et al.* [52] who investigated *post-mortem* the directional solidification of bulk hypo- and hyper-eutectic Al-Cu alloy. Although purely diffusive conditions were not achieved during the present work, the horizontal solidification experiments can be considered as reference cases for the comparison with the two vertical configurations. Indeed, in horizontal configuration buoyancy effects were strongly minimized by the confinement of the grain flotation in the small thickness of the sample. Thus, the grain motion was significantly restricted as reported in [24, 37] and numerically studied by [53]. In a same way, thermally and solutally induced convection was also expected to be significantly limited,

409 as previously discussed by Nguyen-Thi et al. using an order of magnitude analysis [50].

410 During the upward solidification experiments, the present observations show that the grain
411 structure formation was disturbed mainly by the grain flotation due to buoyancy. This is at the
412 origin of the non-homogeneous grain structure and wider distribution of the grain size. On one
413 hand, the grains that moved towards the hot part of the sample and then melted did not
414 participate to the final grain structure, thus leaving more space for the development both upward
415 and on the sides of grains that remained stuck in the thickness. As a consequence, both larger
416 and longer grains than in the horizontal case were obtained. It is worth noticing that the melted
417 grains could strongly modify the solute composition of the bulk liquid phase, which for bulk
418 samples such as ingot casting could be at the origin of strong macrosegregation. On the other
419 hand, the growth of grains that nucleated in the residual liquid areas was restricted by the
420 previously stuck grains, which resulted in the occurrence of smaller grains than in the horizontal
421 case. The same went for the grains originating from dendrite fragments.

422 It is worth noting that buoyancy effects became negligible with the increase of cooling rate
423 [47, 54]. Indeed, for a cooling rate of about 0.9 K/s (not shown in this paper), the growth
424 velocity (~ 120 µm/s) and the grain flotation velocity (~ 100 µm/s) were of same order, yielding
425 to an attenuation of the impact of flotation. Indeed, grains didn’t have enough time to move
426 upward after nucleation due to the rapid nucleation of a new layer of grains blocking their
427 motion, leading the development of a grain structure similar to the one obtained in the horizontal
428 case.

A visually striking feature of the downward experiments is the downward flows of Cu-rich liquid leading the formation of solute plumes that were continuously drifting along the effective solidification front. This non-stationary behavior may be attributed to the local change of the grain structure and its permeability during the growth process, yielding to a modification of the dissipative drag force exerted on the liquid and thus on the solute plumes [55]. Similar observations were also reported by Copley *et al.* [56] or Hellawell *et al.* [57] in transparent alloys, Hachani *et al.* [58] for Sn-3wt.%Pb alloy and more recently by Boden *et al.* [59] and Shevchenko *et al.* [32] during upward vertical solidification of Ga-In samples or Nelson *et al.* [51] during downward solidification of Al-Cu alloys.

The close link between dendrite tip velocity and solute plume motion ahead of the dendrite tip (Fig. 8) has been already mentioned by Shevchenko *et al.* [32] for the study of Ga-In, and more recently by Reinhart *et al.* [60] during directional solidification of superalloys. The explanation for these cycles running concurrently is that solute plumes locally increased the Cu concentration ahead of the dendrite tip, which reduced the constitutional undercooling intensity and thus slowed the dendrite tip growth [61].

By comparing the grain size orientation distributions of the three cases, it appears that the effect of the temperature gradient and of gravity on the grain morphology was stronger during downward experiments than for horizontal or upward experiments. During downward directional solidification of refined alloys, gravity impacts the grain structure dynamics by three distinct mechanisms. Firstly, there is the local increase of solute composition ahead of the

449 solidification front due to the solute plumes that reduces the constitutional undercooling
450 intensity in front of the equiaxed structure. This modifies not only the dendrite tip velocity as
451 discussed above but also provoked an inhibition of refiners. As a result, no nucleation of new
452 grains was observed in the close vicinity of the solute plumes and the already existing grains
453 have become more elongated. We can also mention that solute plumes could also change the
454 spatial distribution of refining particles. However, this effect could not be analyzed in our
455 experiments. Secondly, a subtler effect of gravity on grain structure formation is caused by the
456 sinking of the Cu-enriched liquid, which stretches the solute boundary. The dilation of iso-
457 concentrations has been also put forward by Bogno *et al.* [62] to explain the difference in
458 behavior, in terms of velocity and length, of the upward and downward arms of equiaxed grains
459 growing in isothermal conditions but in a vertical sample. Consequently, liquid undercooling
460 ahead of the existing grain structure becomes less intense, yielding to a reduction of the grains
461 nucleation rate and then augmenting the growth period. A third effect comes from the fact that
462 the grains did not nucleate directly in front of the growing dendrite tips, but often appeared on
463 their sides. Those grains moved toward the solidification front due to buoyancy effect and were
464 trapped in the mushy zone, in between grains that were already developing. The consequence
465 of these combined effects was that long grains of several millimeters could easily develop
466 toward the bottom of the FoV without being blocked, while the growth of grains trapped in the
467 mushy zone was stopped, which agrees well with the measurement of both small equiaxed
468 grains and long columnar dendrites as shown in Fig. 9.

Finally, it can be mentioned that the formation of segregated channels in the mushy zone was not observed in our experiments as (*i*) either the secondary arms of dendrites on both sides of the plumes grew more rapidly than the average transport of solute or (*ii*) free equiaxed grains moved upward and plugged the root of the plumes (see Supplementary Video 3). Only a residual liquid area developed above the porosity (Fig. 7d) and lead the formation of a segregated area. For a sake of completeness, we can mention that stable liquid channels on one side of the sample were observed during downward solidification of refined Al-20wt.%Cu alloys with the application of permanent magnetic field [63]. In those experiments, it has been demonstrated that an additional thermo-electro-magnetic force pushes the Cu-enriched liquid in the transverse direction of the sample. As a result, a liquid channel was created on one side of the sample, depending on the magnetic field direction.

7. Conclusion

Gravity effects on equiaxed solidification were investigated during horizontal, vertical upward and vertical downward directional solidifications of refined Al-20wt.%Cu (0.1wt.% AlTiB) samples. The solidification has been provoked by lowering the temperature of both heater elements and the observation of the grain structure has been done *in situ* and in real-time by X-radiography using the SFINX laboratory facility. The comparison between the three experimental configurations enlightened the marked effects of gravity on the grain structure formation and then on the final grain structure:

- For upward solidification, the dominant effect was buoyancy that provoked the grain flotation in the case of Al-20wt.%Cu alloy and caused the formation of liquid pockets at low growth rates. The grain motion following the nucleation phase yielded a non-homogeneous grain structure.
- For downward solidification, the most striking effect was the formation of solute flow, also called solute plumes. These fluid flows strongly affected the dendrite growth kinetic, which oscillated in phase with solute variations in the liquid ahead of the dendrite tips. Moreover, the local increase in solute due to the plumes prevented grain nucleation in their close vicinity. Another influence of gravity is related to buoyancy that kept the grains very close to the downward growing microstructure and then significantly shortened their growth duration. As a result, the average grain size was three times smaller for this type of experiment than for horizontal or upward solidifications.

All these gravity-driven effects have been observed only at low growth rates. For higher growth rates, neither grain flotation nor solute plume movement affected the microstructure.

To continue the study and overcome the gravity effects, a microgravity solidification experiment was conducted on board of the sounding rocket MASER-14 in June 2019 to obtain benchmark experimental data. The columnar-to-equiaxed transition was investigated during this campaign, for a grain-refined Al-20wt.%Cu sample, which is also the alloy composition used in this paper. A comparison will be made between the experiments carried out in microgravity and on ground, as the one presented in this paper, to investigate further the impact

of gravity and allow a reliable comparison with numerical simulations.

Acknowledgements

This work is supported by the XRMON project (AO-2004-046) of the MAP program of the European Space Agency (ESA), by the French National Space Agency (CNES) and the French-Algerian doctoral fellowship program PROFAS B+. The authors would also like to thank the Swedish Space Corporation (SSC) for the development of the SFINX facility and the technical support.

Appendix A. Supplementary data

Supplementary data related to this article can be found at (link to supplementary material)

References

[1] T.E. Quested, Understanding mechanisms of grain refinement of aluminium alloys by inoculation, Materials Science and Technology 20(11) (2004) 1357-1369.

[2] J.A. Spittle, Columnar to equiaxed grain transition in as solidified alloys, Int. Mater. Rev. 51(4) (2006) 247-269.

[3] M.D. Dupouy, B. Drevet, D. Camel, Influence of Convection on the Selection of Solidification Microstructures at Low Growth Rates, J. Cryst. growth 181 (1997) 145-159.

[4] S.R. Coriell, M.R. Cordes, W.J. Boettinger, R.F. Sekerka, Convective and interfacial instabilities during unidirectional solidification of a binary alloy, Journal of Crystal Growth 49(1) (1980) 13-28.

[5] G.B. McFadden, R.G. Rehm, S.R. Coriell, W. Chuck, K.A. Morrish, Thermosolutal Convection During Directional Soliidification, Metallurgical Transactions a-Physical Metallurgy and Materials Science 15(12) (1984) 2125-2137.

[6] M.E. Glicksman, S.R. Coriell, G.B. McFadden, Interaction of flows with the crystal-melt interface, Ann. Rev. Fluid Mech. 18 (1986) 307.

[7] S.H. Davis, Hydrodynamics Interactions in Directional Solidification, J. Fluid Mech. 212 (1990) 241-262.

[8] S. Akamatsu, H. Nguyen-Thi, In situ observation of solidification patterns in diffusive conditions, Acta Mater. 108 (2016) 325-346.

[9] M.H. Burden, D.J. Hebditch, J.D. Hunt, Macroscopic Stability of a planar, cellular or dendritic interface during

directional freezing, J. Cryst. Growth 20 (1973) 121-124.
[10] H. Nguyen-Thi, Y. Dabo, B. Drevet, M.D. Dupouy, D. Camel, B. Billia, J.D. Hunt, A. Chilton, Directional Solidification of Al-1.5wt% Ni alloys under diffusion transport in space and fluid flow localisation on Earth, J. of Crystal Growth 281 (2005) 654-668.
[11] J.D. Verhoeven, J.T. Mason, R. Trivedi, The Effect of Convection on the Dendrite to Eutectic Transition, Metall. Trans. A 17A (1986) 991-1000.
[12] A. Bogno, G. Reinhart, A. Buffet, H. Nguyen Thi, B. Billia, T. Schenk, N. Mangelinck-Noël, N. Bergeon, J. Baruchel, In situ analysis of the influence of convection during the initial transient of planar solidification, Journal of Crystal Growth 318(1) (2011) 1134-1138.
[13] A. Bogno, H. Nguyen-Thi, A. Buffet, G. Reinhart, B. Billia, N. Mangelinck-Noël, N. Bergeon, J. Baruchel, T. Schenk, Analysis by synchrotron X-ray radiography of convection effects on the dynamic evolution of the solid-liquid interface and on solute distribution during the initial transient of solidification, Acta Mater. 59(11) (2011) 4356-4365.
[14] H. Jamgotchian, B. Billia, L. Capella}, Interaction of thermal convection with the solid-liquid interface during downward solidification of Pb-30wt\%Tl alloys, J. of Crystal Growth 85(3) (1987) 318-326.
[15] H. Nguyen-Thi, A. Bogno, G. Reinhart, B. Billia, R.H. Mathiesen, G. Zimmermann, Y. Houltz, K. Löth, D. Voss, A. Verga, F.d. Pascale, Investigation of gravity effects on solidification of binary alloys with in situ X-ray radiography on earth and in microgravity environment, Journal of Physics: Conference Series 327(1) (2011) 012012.
[16] G. Reinhart, H. Nguyen Thi, J. Gastaldi, B. Billia, N. Mangelinck-Noël, T. Schenk, J. Härtwig, J. Baruchel, In situ and real time investigation of directional solidification
of Al - Ni alloys by synchrotron imaging, Materials Science Forum 508 (2006) 75-80.
[17] H. Nguyen-Thi, G. Reinhart, G.S. Abou Jaoude, R.H. Mathiesen, G. Zimmermann, Y. Houltz, D. Voss, A. Verga, D.J. Browne, A.G. Murphy, XRMON-GF: A novel facility for solidification of metallic alloys with in situ and time-resolved X-ray radiographic characterization in microgravity conditions, Journal of Crystal Growth 374 (2013) 23-30.
[18] G. Reinhart, H. Nguyen-Thi, N. Mangelinck-Noel, J. Baruchel, B. Billia, In Situ Investigation of Dendrite Deformation During Upward Solidification of Al-7wt.%Si, JOM 66(8) (2014) 1408-1414.
[19] A.G. Murphy, G. Reinhart, H. Nguyen-Thi, G.S. Abou Jaoude, D.J. Browne, Meso-scale modelling of directional solidification and comparison with in situ X-ray radiographic observations made during the MASER-12 XRMON microgravity experiment, Journal of Alloys and Compounds 573 (2013) 170-176.
[20] F.L. Mota, N. Bergeon, D. Tourret, A. Karm, R. Trivedi, B. Billia, Initial transient behavior in directional solidification of a bulk transparent model alloy in a cylinder, Acta Mater. 85 (2015) 362-377.
[21] D.R. Liu, N. Mangelinck-Noel, C.A. Gandin, G. Zimmermann, L. Sturz, H. Nguyen-Thi, B. Billia, Simulation of directional solidification of refined Al-7 wt.%Si alloys - Comparison with benchmark microgravity experiments, Acta Mater. 93 (2015) 24-37.
[22] D.R. Liu, N. Mangelinck-Noel, C.A. Gandin, G. Zimmermann, L. Sturz, H.N. Thi, B. Billia, Structures in directionally solidified Al-7 wt.% Si alloys: Benchmark experiments under microgravity, Acta Mater. 64 (2014) 253-265.
[23] Y.Z. Li, N. Mangelinck-Noël, G. Zimmermann, L. Sturz, H. Nguyen-Thi, Comparative study of directional solidification of Al-7 wt% Si alloys in Space and on Earth: Effects of gravity on dendrite growth and Columnar-to-

equiaxed transition, Journal of Crystal Growth 513 (2019) 20-29.
[24] A.G. Murphy, R.H. Mathiesen, Y. Houltz, J. Li, C. Lockowandt, K. Henriksson, G. Zimmermann, N. Melville, D.J. Browne, XRMON-SOL: Isothermal equiaxed solidification of a grain refined Al–20 wt%Cu alloy, Journal of Crystal Growth 440 (2016) 38-46.
[25] J. Baruchel, M. Di Michiel, T. Lafford, P. Lhuissier, J. Meyssonnier, H. Nguyen-Thi, A. Philip, P. Pernot, L. Salvo, M. Scheel, Synchrotron X-ray imaging for crystal growth studies, Comptes Rendus Physique 14(2–3) (2013) 208-220.
[26] R.H. Mathiesen, L. Arnberg, H. Nguyen-Thi, B. Billia, In Situ X-Ray Video Microscopy as a Tool in Solidification Science, JOM 64(1) (2012) 76-82.
[27] L. Abou-Khalil, J. Wang, G. Salloum-Abou-Jaoude, M. Garrido, X. Li, Z. Ren, G. Reinhart, H. Nguyen-Thi, Y. Fautrelle, Investigation of Thermo-Electro-Magnetic force on equiaxed grain motion during upward directional solidification, International Journal of Thermal Sciences 145 (2019) 106047.
[28] G. Salloum-Abou-Jaoude, H. Nguyen-Thi, G. Reinhart, R.H. Mathiesen, G. Zimmermann, D. Voss, Characterization of motion of dendrite fragment by X-ray radiography on Earth and under microgravity environment
Materials Science Forum 790-791 (2014) 311-316.
[29] A.G. Murphy, W.U. Mirihanage, D.J. Browne, R.H. Mathiesen, Equiaxed dendritic solidification and grain refiner potency characterised through in situ X-radiography, Acta Mater. 95 (2015) 83-89.
[30] A. Bogno, H. Nguyen-Thi, B. Billia, G. Reinhart, N. Mangelinck-Noel, N. Bergeon, T. Schenk, J. Baruchel, Iop, In situ and real-time analysis of the growth and interaction of equiaxed grains by synchrotron X- ray radiography, 3rd International Conference on Advances in Solidification Processes, Iop Publishing Ltd, Bristol, 2012.
[31] M. Becker, S. Klein, F. Kargl, In-situ solute measurements with a laboratory polychromatic microfocus X-ray source during equiaxed solidification of an Al-Ge alloy, Scr. Mater. 124 (2016) 34-37.
[32] N. Shevchenko, O. Roshchupkina, O. Sokolova, S. Eckert, The effect of natural and forced melt convection on dendritic solidification in Ga-In alloys, Journal of Crystal Growth 417 (2015) 1-8.
[33] M. Becker, C. Dreissgacker, S. Klein, F. Kargl, Near-isothermal furnace for in situ and real time X-ray radiography solidification experiments, Review of Scientific Instruments 86(6) (2015).
[34] A.G. Murphy, D.J. Browne, W.U. Mirihanage, R.H. Mathiesen, Combined in situ X-ray radiographic observations and post-solidification metallographic characterisation of eutectic transformations in Al-Cu alloy systems, Acta Mater. 61(12) (2013) 4559-4571.
[35] C. Rakete, C. Baumbach, A. Goldschmidt, D. Samberg, C.G. Schroer, F. Breede, C. Stenzel, G. Zimmermann, C. Pickmann, Y. Houltz, C. Lockowandt, O. Svenonius, P. Wiklund, R.H. Mathiesen, Compact x-ray microradiograph for in situ imaging of solidification processes: Bringing in situ x-ray micro-imaging from the synchrotron to the laboratory, Review of Scientific Instruments 82(10) (2011).
[36] L. Abou-Khalil, G. Salloum-Abou-Jaoude, G. Reinhart, C. Pickmann, G. Zimmermann, H. Nguyen-Thi, Influence of gravity level on Columnar-to-Equiaxed Transition during directional solidification of Al – 20 wt.% Cu alloys, Acta Mater. 110 (2016) 44-52.
[37] D.J. Browne, F. Garcia-Moreno, H. Nguyen-Thi, G. Zimmermann, F. Kargl, R.H. Mathiesen, A. Griesche, O. Minster, Overview of In Situ X-Ray Studies of Light Alloy Solidification in Microgravity, in: K.N. Solanki, D. Orlov, A. Singh, N.R. Neelameggham (Eds.), Magnesium Technology 2017, Springer International Publishing Ag, Cham, 2017, pp. 581-590.

618 [38] A. Buffet, H. Nguyen Thi, A. Bogno, T. Schenk, N. Mangelinck-Noël, G. Reinhart, N. Bergeon, B. Billia, J.
619 Baruchel, Measurement of solute profiles by means of synchrotron X-ray radiography during directional
620 solidification of Al - 4 wt% Cu alloys, Materials Science Forum 649 (2010) 331-336.
621 [39] H. Soltani, G. Reinhart, M.C. Benoudia, F. Ngomesse, M. Zahzouh, H. Nguyen-Thi, Impact of growth velocity
622 on grain structure formation during directional solidification of a refined Al-20 wt.%Cu alloy, Journal of Crystal
623 Growth 548 (2020) 125819.
624 [40] A.L. Greer, A.M. Bunn, A. Tronche, P.V. Evans, D.J. Bristow, Modelling of inoculation of metallic melts:
625 application to grain refinement of aluminium by Al-Ti-B, Acta Mater. 48(11) (2000) 2823-2835.
626 [41] M. Abramoff, P. Magalhães, S.J. Ram, Image Processing with ImageJ, Biophotonics International 11 (2003)
627 36-42.
628 [42] V.B. Biscuola, M.A. Martorano, Mechanical Blocking Mechanism for the Columnar to Equiaxed Transition,
629 Metallurgical and Materials Transactions a-Physical Metallurgy and Materials Science 39A(12) (2008) 2885-2895.
630 [43] H. Nguyen-Thi, G. Reinhart, N. Mangelinck-Noël, H. Jung, B. Billia, T. Schenk, J. Gastaldi, J. Härtwig, J. Baruchel,
631 In-Situ and Real-Time Investigation of Columnar-to-Equiaxed Transition in Metallic Alloy, Metallurgical and
632 Materials Transactions A 38(7) (2007) 1458-1464.
633 [44] A. Prasad, S.D. McDonald, H. Yasuda, K. Nogita, D.H. StJohn, A real-time synchrotron X-ray study of primary
634 phase nucleation and formation in hypoeutectic Al–Si alloys, Journal of Crystal Growth 430 (2015) 122-137.
635 [45] Y.J. Xu, D. Casari, R.H. Mathiesen, Y.J. Li, Revealing the heterogeneous nucleation behavior of equiaxed grains
636 of inoculated Al alloys during directional solidification, Acta Mater. 149 (2018) 312-325.
637 [46] Y. Jia, D. Wang, Y. Fu, A. Dong, G. Zhu, D. Shu, B. Sun, In situ Investigation of the Heterogeneous Nucleation
638 Sequence in Al-15 Weight Percent Cu Alloy Inoculated by Al-Ti-B, Metallurgical and Materials Transactions A 50(4)
639 (2019) 1795-1804.
640 [47] H. Soltani, G. Reinhart, M.C. Benoudia, M. Zahzouh, H. Nguyen-Thi, Impact of gravity-related phenomena on
641 the grain structure formation: comparative study between horizontal and vertical solidification of a refined Al-
642 20wt.%Cu alloy, IOP Conference Series: Materials Science and Engineering 529 (2019) 012019.
643 [48] J.D. Hunt, Steady State Columnar and Equiaxed Growth of Dendrites and Eutectic, Materials Science and
644 Engineering 65 (1984) 75-83.
645 [49] S. Ganesan, D.R. Poirier, Densities of Aluminum-Rich Aluminum-Copper Alloys during Solidification,
646 Metallurgical Transaction A 18A (1987) 721-723.
647 [50] H. Nguyen-Thi, G. Reinhart, G. Salloum-Abou-Jaoude, D.J. Browne, A.G. Murphy, Y. Houltz, J. Li, D. Voss, A.
648 Verga, R.H. Mathiesen, G. Zimmermann, XRMON-GF Experiments Devoted to the in Situ X-ray Radiographic
649 Observation of Growth Process in Microgravity Conditions, Microgravity Science and Technology 26(1) (2014) 37-
650 50.
651 [51] T. Nelson, B. Cai, N. Warnken, P.D. Lee, E. Boller, O.V. Magdysyuk, N.R. Green, Gravity effect on thermal-solutal
652 convection during solidification revealed by four-dimensional synchrotron imaging with compositional mapping,
653 Scr. Mater. 180 (2020) 29-33.
654 [52] M.D. Dupouy, D. Camel, J.J. Favier, Natural convective effects in directional dendritic solidification of binary
655 metallic alloys: dendritic array morphology, Journal of Crystal Growth 126(2–3) (1993) 480-492.
656 [53] A. Olmedilla, M. Zaloznik, H. Combeau, Quantitative 3D mesoscopic modeling of grain interactions during
657 equiaxed dendritic solidification in a thin sample, Acta Mater. 173 (2019) 249-261.

[54] G. Zimmermann, C. Pickmann, M. Hamacher, E. Schaberger-Zimmermann, H. Neumann-Heyme, K. Eckert, S. Eckert, Fragmentation-driven grain refinement in directional solidification of AlCu10wt-% alloy at low pulling speeds, Acta Mater. 126 (2017) 236-250.
[55] A. Saad, C.-A. Gandin, M. Bellet, N. Shevchenko, S. Eckert, Simulation of Channel Segregation During Directional Solidification of In—75 wt pct Ga. Qualitative Comparison with In Situ Observations, Metallurgical and Materials Transactions A 46(11) (2015) 4886-4897.
[56] S.M. Copley, A.F. Giamei, S.M. Johnson, M.F. Hornbecker, The origin of freckles in unidirectionally solidified castings, Metallurgical Transactions 1(8) (1970) 2193-2204.
[57] A. Hellawell, J.R. Sarazin, R.S. Steube, Channel Convection in Partly Solidified Sustems, Philosophical Transactions of the Royal Society of London Series a-Mathematical Physical and Engineering Sciences 345(1677) (1993) 507-544.
[58] L. Hachani, B. Saadi, X.D. Wang, A. Nouri, K. Zaidat, A. Belgacem-Bouzida, L. Ayouni-Derouiche, G. Raimondi, Y. Fautrelle, Experimental analysis of the solidification of Sn–3 wt.%Pb alloy under natural convection, International Journal of Heat and Mass Transfer $V 55 (7) (2012) 1986-1996.
[59] S. Boden, S. Eckert, G. Gerbeth, Visualization of freckle formation induced by forced melt convection in solidifying GaIn alloys, Materials Letters 64(12) (2010) 1340-1343.
[60] G. Reinhart, D. Grange, L. Abou-Khalil, N. Mangelinck-Noël, N.T. Niane, V. Maguin, G. Guillemot, C.A. Gandin, H. Nguyen-Thi, Impact of solute flow during directional solidification of a Ni-based alloy: In-situ and real-time X-radiography, Acta Mater. 194 (2020) 68-79.
[61] L. Yuan, P.D. Lee, A new mechanism for freckle initiation based on microstructural level simulation, Acta Mater. 60(12) (2012) 4917-4926.
[62] A. Bogno, H. Nguyen-Thi, G. Reinhart, B. Billia, J. Baruchel, Growth and interaction of dendritic equiaxed grains: In situ characterization by synchrotron X-ray radiography, Acta Mater. 61(4) (2013) 1303-1315.
[63] Y. Fautrelle, J. Wang, G. Salloum-Abou-Jaoude, L. Abou-Khalil, G. Reinhart, X. Li, Z. Ren, H. Nguyen-Thi, Thermo-Electric-Magnetic Hydrodynamics in Solidification: In Situ Observations and Theory, JOM Journal of the Minerals, Metals and Materials Society 70(5) (2018) 764 - 771.

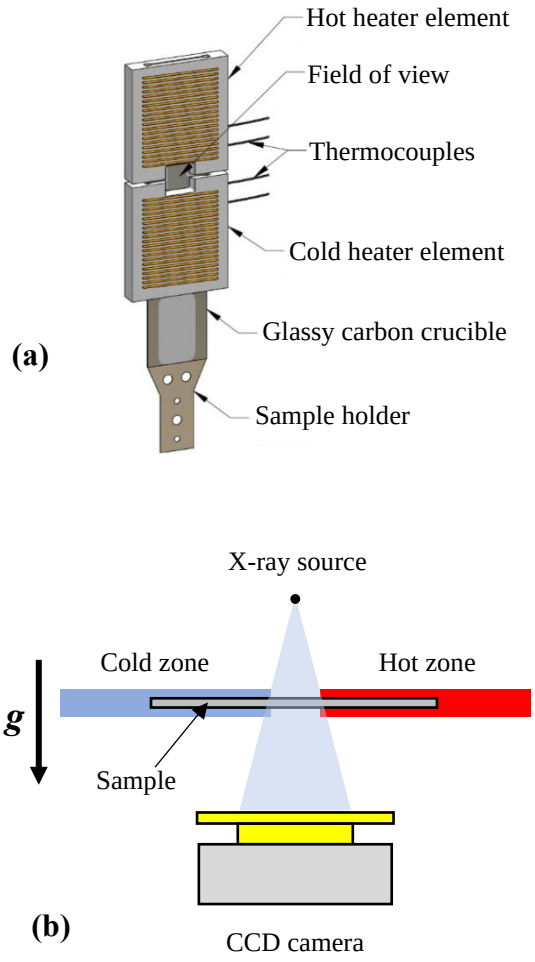

Fig. 1: Schematic layout of (a) the SFINX furnace (courtesy of A. G. Murphy, UCD), and (b) the SFINX experimental arrangement (furnace and X-radiography system) for horizontal solidification experiment.

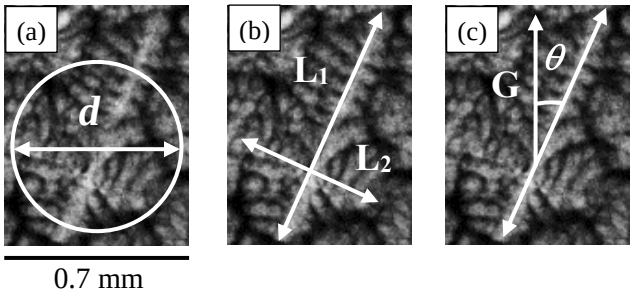

Fig. 2: Dendritic grain characteristics measured in the present paper: (a) Diameter d of the equivalent disk, (b) L_1 length of the longest straight segment in the grain and L_2 length of the longest straight segment in the grain and orthogonal to the segment L_1, (c) tilt angle θ between the temperature gradient direction and the main dendrite axis.

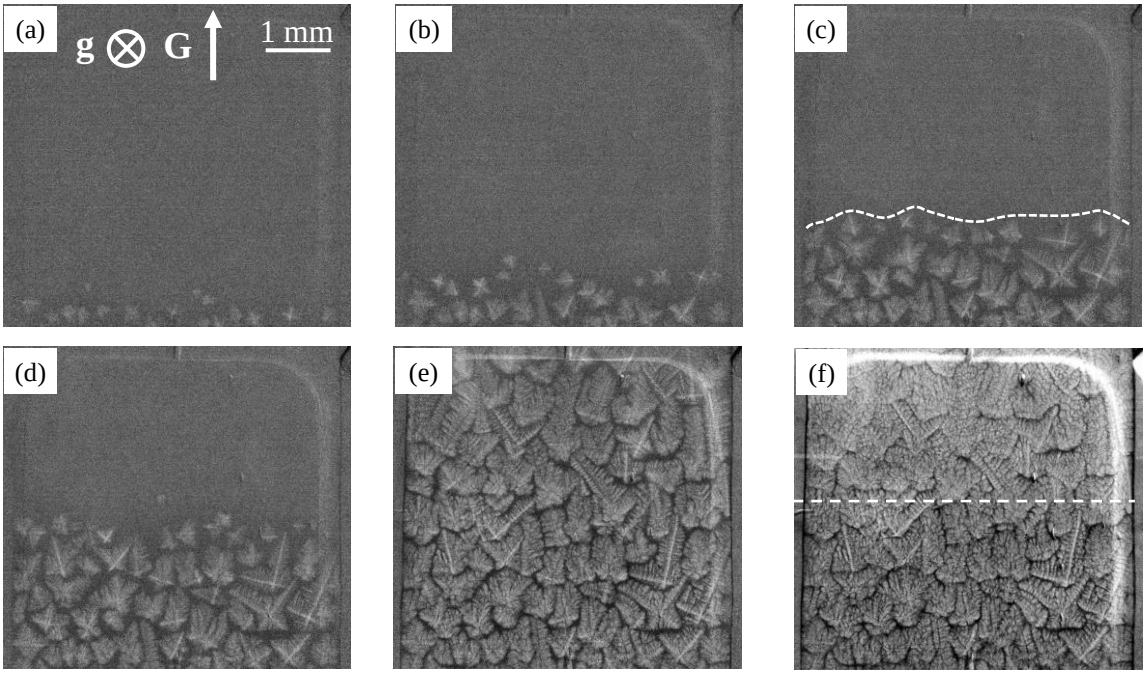

Fig. 3: Sequence of radiographs recorded during the solidification experiment A1 (refined Al-20wt.%Cu in horizontal configuration, $\langle V_N \rangle$ = 25.4 µm/s and $\langle G_N \rangle$ = 5.9 K/mm), showing the propagation of the solidification microstructure. (The reference time t = 0 s is chosen at the beginning of the temperature decrease: a) t = 135 s, b) t = 151 s, c) t = 179 s (the dashed line points out the effective solidification front), d) t = 202 s, e) t = 337s, f) t = 562 s (the dashed line shows the eutectic front crossing the Field-of-View).

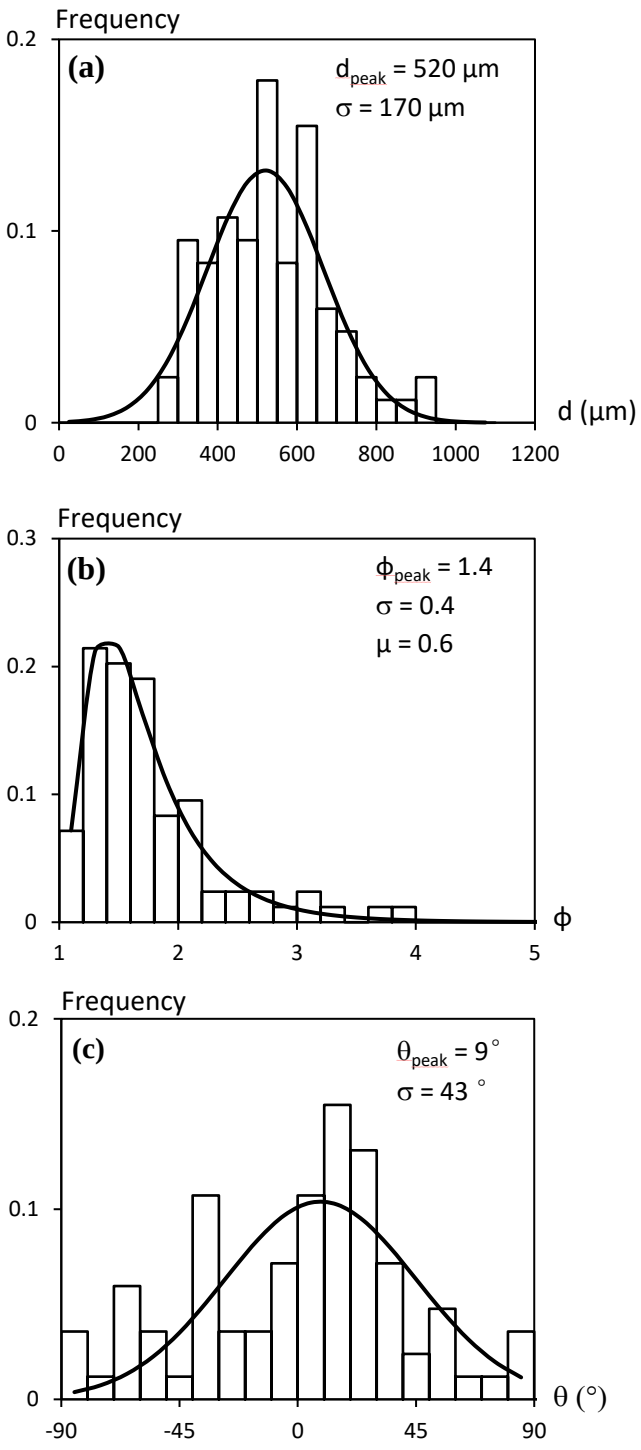

Fig. 4: Distributions of (a) grain size, (b) grain elongation and (c) growth orientation for the experiment A1 (horizontal solidification of a refined Al-20wt.%Cu, $<V_N>$ = 25.4 µm/s and $<G_N>$ = 5.9 K/mm).

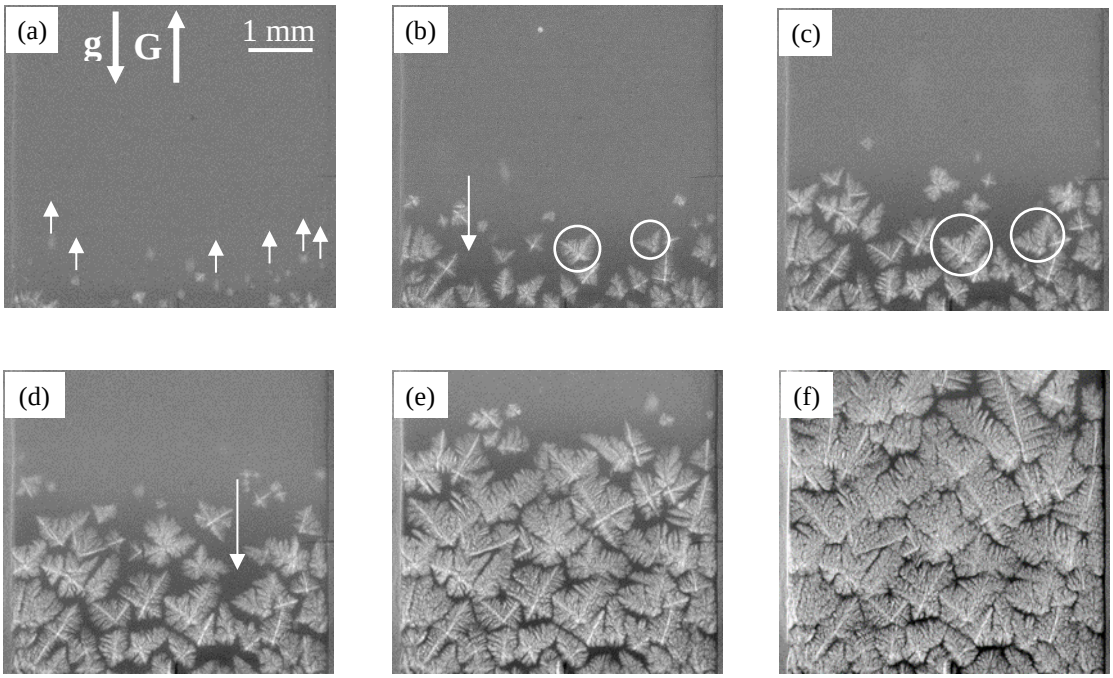

Fig. 5: Sequence of radiographs recorded during the upward solidification B2 (refined Al-20 wt.%Cu, $<V_N>$ = 23.4µm/s and $<G_N>$ = 6.4 K/mm). The reference time t = 0 s is chosen at the beginning of the temperature decrease: a) t = 13 s (upward white arrows indicate the motion of the grains) , b) t = 30 s (the downward white arrow indicates a residual liquid area formed between grains and white circles show two stuck grains), c) t = 47 s (white circles show two stuck grains), d) t = 58 s (the downward white arrow indicates a residual liquid area formed between grains), e) t = 92 s, f) t = 153 s.

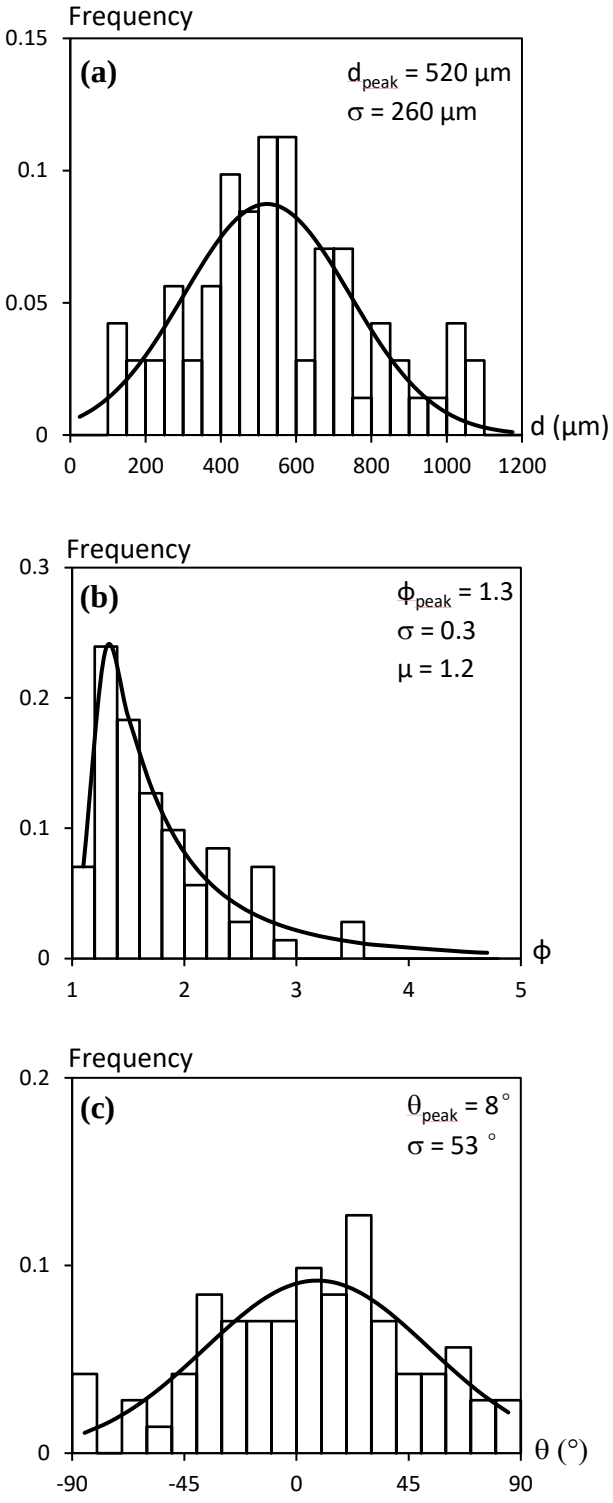

Fig. 6: Distributions of (a) grain size, (b) grain elongation and (c) growth orientation for the vertical upward configuration in the B2 case (refined Al-20wt.%Cu, $\langle V_N \rangle$ = 23.4 µm/s and $\langle G_N \rangle$ = 6.4 K/mm).

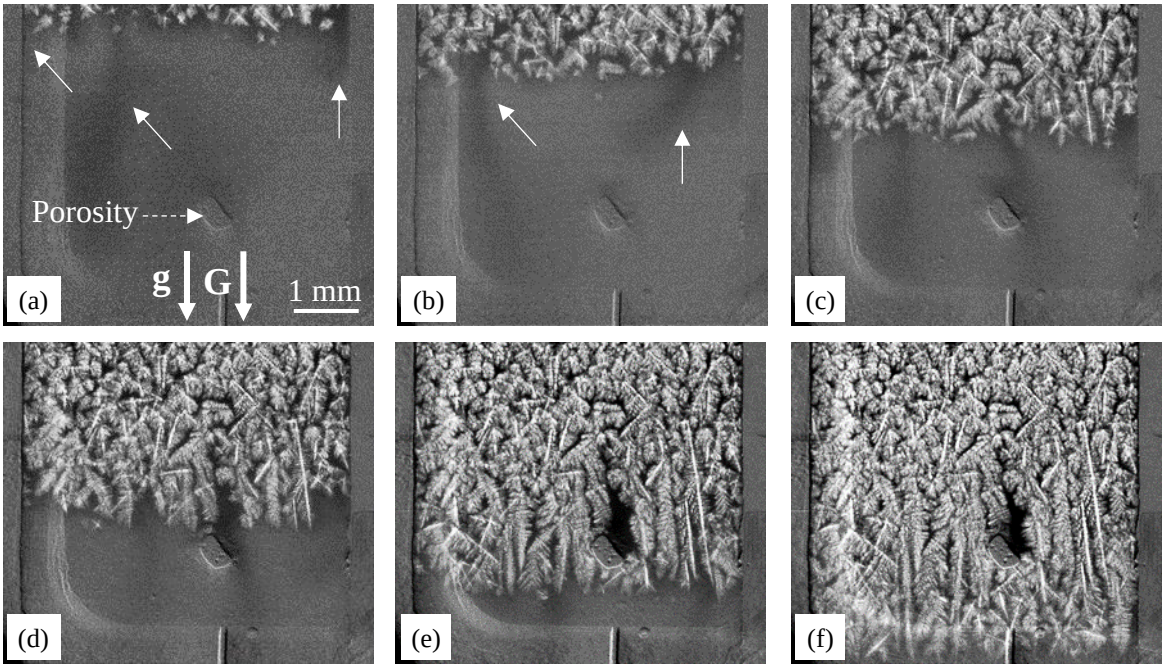

Fig. 7: Sequence of radiographs recorded during the experiment C1 (downward solidification of a refined Al-20wt.%Cu, $\langle V_N \rangle$ = 22.2 µm/s and $\langle G_N \rangle$ = 6.8 K/mm), showing the propagation of the solidification microstructure from the top-cold zone toward the bottom-hot zone of the sample. The plain white arrows show solute plume locations. The reference time t = 0 s is chosen at the beginning of the temperature decrease: a) t = 175 s, b) t = 218 s, c) t = 280 s, d) t = 333 s, e) t = 420 s, f) t = 491 s.

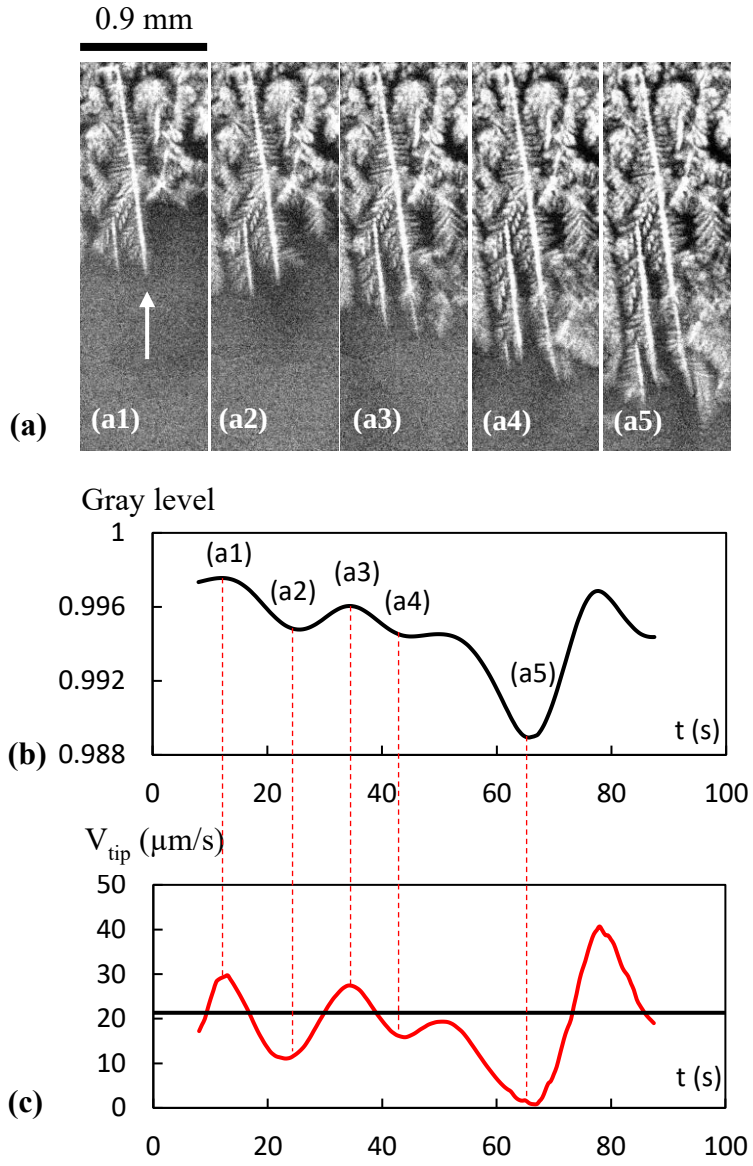

Fig. 8: (a) Sequence of radiographs of a dendrite development during the experiment C1 (downward solidification of a refined Al-20wt.%Cu, $\langle V_N \rangle = 22.2$ µm/s and $\langle G_N \rangle = 6.8$ K/mm) at (a1) $t = 288$ s, (a2) $t = 298$ s, (a3) $t = 311$ s, (a4) $t = 334$s and (a5) $t = 352$ s (the reference time $t = 0$ s is chosen at the beginning of the cooling). (b) Gray level variation in front of the dendrite tip and (c) variation of the tip velocity for the dendrite indicated by a white arrow in the first radiograph.

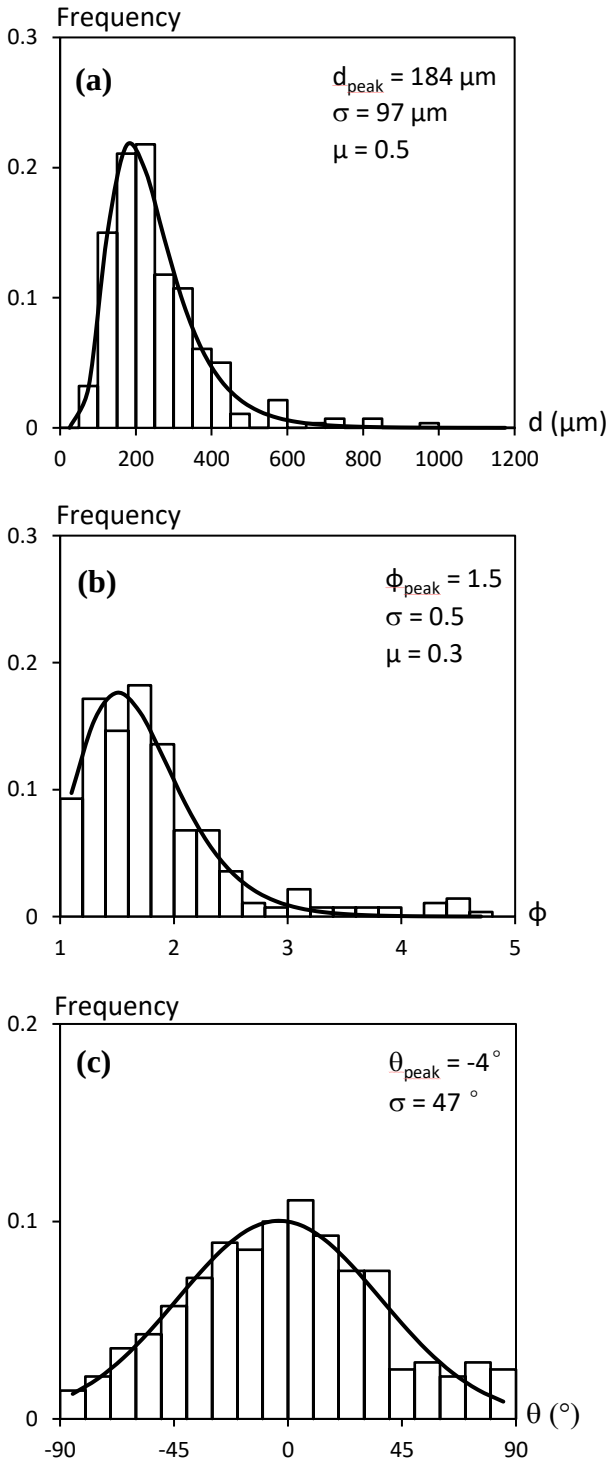

Fig. 9: Distributions of (a) grain size, (b) grain elongation and (c) growth orientation for the C1 experiment (downward solidification of a refined Al-20wt.%Cu, $\langle V_N \rangle$ = 22.2 µm/s and $\langle G_N \rangle$ = 6.8 K/mm).

	Experiment	$<V_N>$ (μm/s)	$<V_E>$ (μm/s)	$<G_N>$ (K/mm)	$<G_E>$ (K/mm)
Case A Horizontal solidification	A1	25.4	27.8	5.9	5.4
	A2	24.5	27.2	6.1	5.5
Case B Upward solidification	B1	24.5	-	6.1	-
	B2	23.4	-	6.4	-
	B3	23.9	-	6.3	-
	B4	22.9	26.5	6.6	5.7
	B5	23.3	27.6	6.4	5.4
	B6	25.7	29.1	5.8	5.2
Case C Downward solidification	C1	22.2	24.7	6.8	6.1
	C2	22.3	24.5	6.7	6.1
	C3	20.2	24.4	7.4	6.1

Table 1 Measured average values of the nucleation front velocity $<V_N>$, eutectic front velocity $<V_E>$, nucleation temperature gradient $<G_N>$ and eutectic temperature gradient $<G_E>$ for the three series of solidification experiment on refined Al-20wt.%Cu alloys.